

WARM NEUTRAL HALOS AROUND MOLECULAR CLOUDS. V. OH (1665 AND 1667 MHz) OBSERVATIONS

PETER G. WANNIER,¹ B-G ANDERSSON,¹ S. R. FEDERMAN,^{1, 2} B. M. LEWIS,³ Y. P. VIALA,⁴ AND E. SHAYA⁵

Received 1992 January 27; accepted 1992 September 28

ABSTRACT

We have made 10 strip maps of 1665 and 1667 MHz OH emission, traversing the outer boundaries of five molecular clouds. The OH emission is found to be significantly extended relative to CO, implying that OH is to be found in abundance in the partly atomic, partly molecular gas surrounding dense neutral clouds. The fractional OH abundance is calculated using existing H I and CO observations, and detailed source models which include a complete chemistry network and a radiative transfer code. The largest OH abundances are found outside of the CO clouds, especially in those regions thought to be suffused by intense UV radiation. We conclude that the extended OH is formed, not by the exothermic reaction of O with H_3^+ , but by the endothermic reaction, $H^+ + O \rightarrow H + O^+$. The increased importance of the endothermic channel, relative to that assumed in earlier work, results from: (1) larger temperatures and (2) a lower efficiency of H_2 production, resulting in a larger H I column density. This is consistent with, and is in fact predicted by, earlier models based on H I and CO observations alone.

Subject headings: ISM: clouds — ISM: molecules — molecular processes

1. INTRODUCTION

Main-line OH emission has provided the basis for several surveys of interstellar clouds. Emission-line surveys have been performed, for example, by Cudaback & Heiles (1969) and Crutcher (1973) in a total of over 100 dark clouds, establishing a general, positive correlation of the OH emission with H_2CO absorption and visual extinction. An interesting feature pointed out by Crutcher is that the velocity half-widths for OH are generally larger (factor 1.72) than those for H_2CO . Because the total velocity width, and the relative increase in width from H_2CO to OH both exceed what could be attributed to thermal broadening, he tentatively attributes the enhancement to a difference in the spatial distributions of the two molecules, in the sense of OH being found more toward the outer regions of molecular clouds. A more recent, but less extensive survey of nine translucent high-latitude clouds (Magnani & Siskind 1990) has been used to infer a line-of-sight OH/H ratio, falling in the range 10^{-8} – 10^{-7} , in agreement with earlier results by Federman et al. (1987).

The present paper is the fifth in a series of papers dealing with the properties of molecular cloud boundaries. In the first three papers we have presented and discussed the properties of cloud halos as seen in 62 H I (21 cm) and CO ($J = 1-0$ and $J = 2-1$) strip maps of 14 molecular clouds (Wannier, Lichten, & Morris 1983, hereafter Paper I; Wannier et al. 1991, hereafter Paper II; Andersson, Wannier, & Morris 1990, hereafter Paper III). A fourth paper presented a two-dimensional map of H I in the B5 molecular cloud, showing a full H I envelope (Andersson, Roger, & Wannier 1992, hereafter Paper IV). Alto-

gether, these observations indicate that molecular clouds are generally surrounded by warm (~ 100 K) H I gas which is (marginally) optically thick in the 21 cm line. The CO boundary layers are also heated and there is a strong correlation between the CO and H I kinetic temperatures, with heating attributed to photoelectric emission from grains.

OH observations were made toward some of the same boundary regions studied in Paper I. In terms of initial cloud chemistry, the OH radical is fundamental to the formation of molecules in the interstellar medium. It is formed of the two most abundant reactive elements and it plays a key role in the chemistry of interstellar water. Thermal emission in the 1665 and 1667 MHz OH lines (the “main” lines) is weak but measurable and, because it is generally optically thin, yields the OH abundance with a minimum of fuss.

2. OBSERVATIONS

The 18 cm OH data were acquired using the Arecibo 305 m telescope during four observing periods: 1987 October 16–21, 1988 February 26–April 25, 1989 September 13–22, and 1990 April 2–9. The antenna/feed combination yielded a beamsize (FWHM) of $3'.0$, with a prominent (-10 dB) diffraction ring lobe of radius $5'.3$. The antenna gain (and sidelobe level) was essentially constant for zenith angles (ZA) of less than 10° , representing most of the data obtained. Due to vignetting, the system performance degraded at zenith angles greater than 10° , a condition which applies to approximately 10% of the observations. Very few scans with $ZA > 15^\circ$ were used, and none with $ZA > 16^\circ$. A ZA correction factor was applied to data between 10° and 16° , similar to the procedure described in Paper II. During the first two observing periods the receiver consisted of a pair (for each circular polarization) of GaAs FET amplifiers. These were replaced, in the second pair of observing periods by a pair of cooled HEMT amplifiers. Effective system temperatures were typically 40–50 K. By splitting the IF, the 1665 and 1667 MHz lines could be measured simultaneously. The four signals (two lines, two polarizations) were fed into a 2048-channel, 2.5 MHz, 3-level autocorrelator spectrometer split into 512-channel quadrants, yielding a velocity

¹ Jet Propulsion Laboratory, California Institute of Technology, Pasadena, CA 91109.

² Department of Physics and Astronomy, University of Toledo, Toledo, OH 43606.

³ Arecibo Observatory, Arecibo, PR 00613.

⁴ Observatoire de Paris, Section de Meudon, DEMIRM, F-92195 Meudon Principal Cedex, France.

⁵ Department of Physics and Astronomy, University of Maryland, College Park, MD 20742.

TABLE 1
SOURCE LIST

Strip Name ^a	R.A. (1950)	Decl. (1950)	b_{\parallel}	P.A. ^b	v_{LSR}^c (km s ⁻¹)	Edges Crossed	Distance (pc)	References	Map Step (pc)
Per OB2 A (IX)	03 ^h 37 ^m 00 ^s	29°49'36"	-20°	0°	8	1	350	1	0.367
Per OB2 B (V)	03 25 40	28 52 00	-22	0	7	1	350	1	0.367
Per OB2 C (I)	03 13 45	29 36 00	-23	-45	2	1	350	1	0.371
L1551 I	04 27 50	18 00 00	-20	0	6	1	150	2	0.157
L1599 A (II)	05 48 02	07 37 12	-10	-45	10	2	400	3	0.436
L1599 B (I)	05 46 45	07 21 15	-10	-45	10	2	400	3	0.436
S255 I	06 10 01	18 00 00	0.1	0	0	1	2500	4	2.62
S255 II	06 10 01	18 00 00	0.1	90	0	1	2500	4	2.76
Mon filament	06 20 00	03 42 06	-4.6	0	-5	2	500	5	0.524
Mon OB1	06 28 00	13 00 00	1.4	0	1	1	900	6	0.942

^a The nomenclature for the Perseus, L1599 and Monoceros strips are taken from Paper I, where the CO and H I data are presented. The nomenclature for the S255 and L1551 strips are from Paper II. The roman numerals in parentheses give the designation, in Paper II, to those strips taken from Paper I.

^b Position angle: east of north.

^c Approximate CO velocity.

REFERENCES.—(1) Ungerechts & Thaddeus 1987, (2) Elias 1978, (3) Murdin & Penston 1977, (4) Evans et al. 1977, (5) Wannier et al. 1983, (6) Racine 1968.

resolution of 0.22 km s⁻¹. All spectra were acquired in frequency switching mode with typical integration times of 30–60 minutes, yielding rms noise values of 0.04–0.06 K. The source list is given in Table 1, consisting of strips previously mapped in H I and CO (Paper I).

The Per OB2 molecular cloud is part of the large complex in Perseus-Taurus-Auriga, mapped in CO by Ungerechts & Thaddeus (1987, hereafter UT). They adopt a distance of 350 pc, which is used in our analysis. The cloud is situated well out of the Galactic plane ($l, b = 160, -20$) and from the integrated CO emission UT estimate a total mass of $5 \times 10^4 M_{\odot}$. It is the site of high-mass star formation and is associated with the H II regions IC 348 and NGC 1333. Figure 1a (adapted from Baran 1982) shows the approximate location and extension of the OH strip maps. Per OB2 B is located on the southern rim of the cloud, i.e., away from the OB-association, and should therefore not be significantly influenced by it. Per OB2 C, located on the Northwest edge, may have an enhanced UV field. The Per OB2 A strip, also located on the southern edge, has an irregular CO profile in that it seems to pass through a clump beyond the molecular cloud boundary. As a result, we do not present a detailed cloud model for this strip.

L1551 is a dark cloud lying to the southeast of the Perseus cloud, in the Taurus region. It has been extensively studied in both CO (e.g., Snell 1981; Moriarty-Schieven et al. 1987) and H I (e.g., van der Werf et al. 1989). It is an active star-forming cloud, as evidenced by the presence of several T Tauri stars (Strom et al. 1985) as well as by one, and possibly two, bipolar outflows centered on IRS 5 (Strom, Strom, & Vrba 1976; Moriarty-Schieven & Wannier 1991). Elias (1978) estimates the distance to the cloud as 140 pc based on a comparison of star counts, reddening data and the brightness of stars associated with the cloud. This makes it the closest cloud in our present sample. One strip map was made in L1551, extending well beyond the CO cloud edge in the south.

L1599 is a small highly elongated cloud at the southeastern rim of the λ Ori complex (Sharpless 1959; Maddalena & Morris 1987). Our strip traverses the cloud, with the northwest boundary being that adjoining the H II region. In addition to the OB association, low-mass stars have formed recently, as indicated by the presence of a large number of H α emission-line stars (Duerr, Imhoff, & Lada 1982). Following Murdin & Penston (1977) we adopt a distance of 400 pc for the system.

We obtained OH data on two strips traversing this cloud (Fig. 1c). Thus each strip passes through two cloud boundaries, and the two strips together sample four transition regions.

The S255 cloud is in fact a molecular cloud associated with the H II region complex consisting of S254–S257. It has been mapped by Bally (see in Paper II) and Heyer et al. (1989), who derive a total cloud mass of $2.7 \times 10^4 M_{\odot}$. The cloud ($l, b = 192, 0$) is approximately 2.5 kpc distant (Evans, Blair, & Beckwith 1977) and is the site of active high-mass star formation, as evidenced by several H II regions and compact radio sources (see, e.g., Snell & Bally 1986). The present data consist of two strips extending mostly north and west from the molecular peak, located more or less equidistant between the compact H II regions S255 and S257 (Fig. 1d). The S255 II strip passes, in fact, into the visible, extended S254 ionized region.

The Monoceros Filament is a source mapped by Maddalena et al. (1986) who interpret it as a gas streamer from the Orion complex towards the Galactic plane. Based on the association with the Orion B cloud they assign a distance of 500 pc which we use in our analysis. There is no evidence for star formation in this cloud.

The Monoceros OB1 cloud is associated with a young association of the same name, and is the site of active star formation as indicated by the presence of the cluster NGC 2264, the reflection nebula Mon R1 and several molecular outflow sources (Margulis, Lada, & Snell 1988). The molecular cloud is close to the Galactic plane, ($b = 1^{\circ}4, d = 900$ pc; Racine 1968) and as a result its extended H I envelope is not readily distinguishable from the general Galactic emission. Therefore we cannot make a reliable H I model and we do not attempt to derive an OH fractional abundance.

3. RESULTS

For each observed position, the 1665 and 1667 MHz data were co-added and the two polarization states combined. Before combining the two frequencies, an analysis of the 1665/1667 MHz line ratio was made to ascertain that they contained equivalent information. A histogram of the resulting ratios is shown in Figure 2, indicating that the column density can be inferred directly from the line intensities, assuming optically thin emission (see discussion in § 4.1). Accordingly, spectra at the two frequencies were combined by rescaling the 1665 MHz

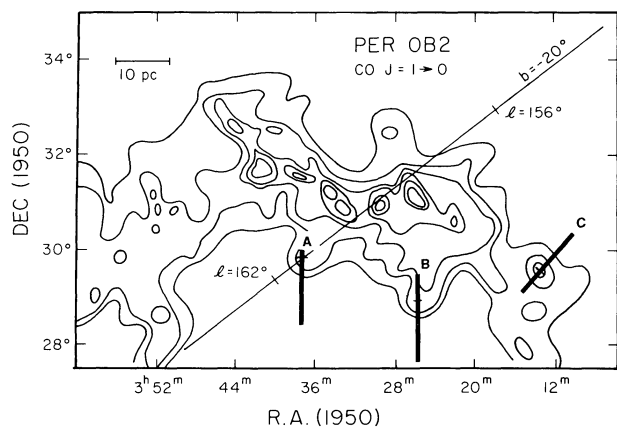


FIG. 1a

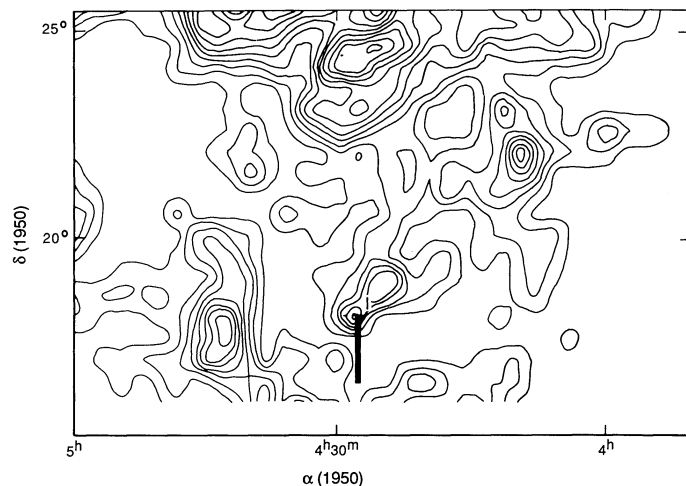


FIG. 1b

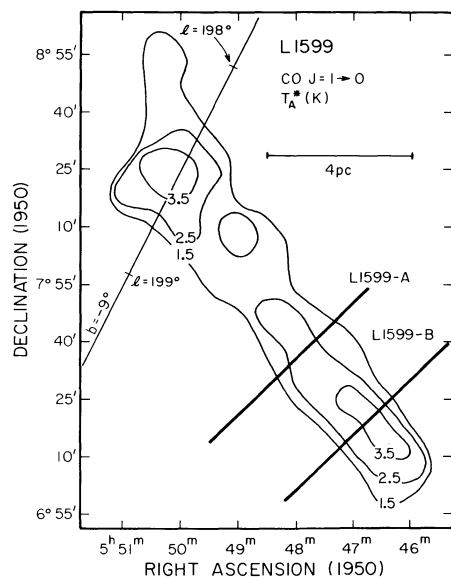


FIG. 1c

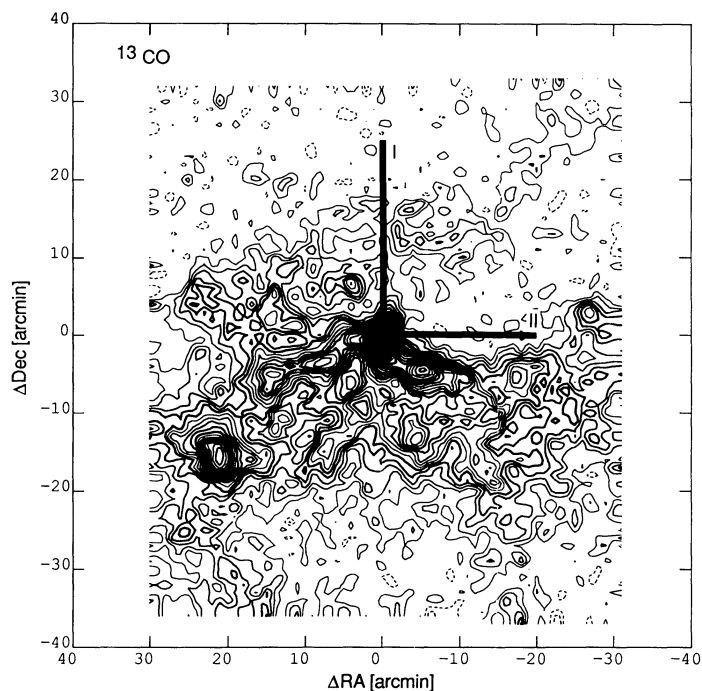


FIG. 1d

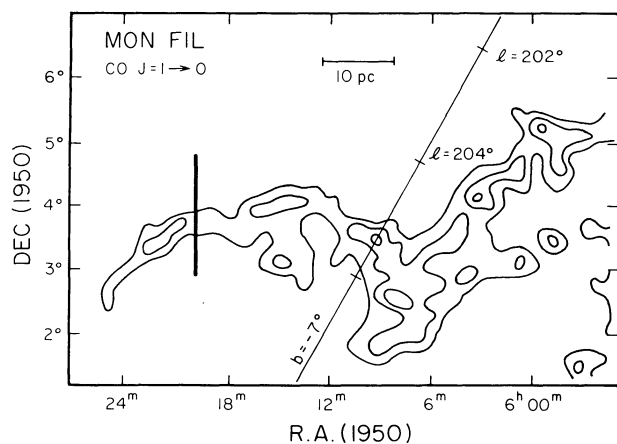


FIG. 1e

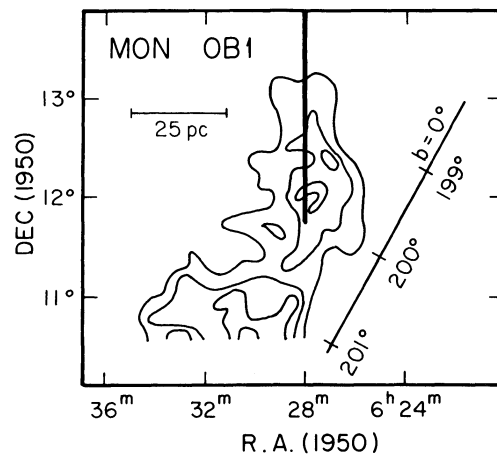


FIG. 1f

FIG. 1.—Locations of the observed OH strip maps are shown relative to maps of the $J = 1-0$ CO line for: (a) Perseus, (b) L1551, (c) L1599, (d) S255, (e) Mon filament, and (f) Mon OB 1.

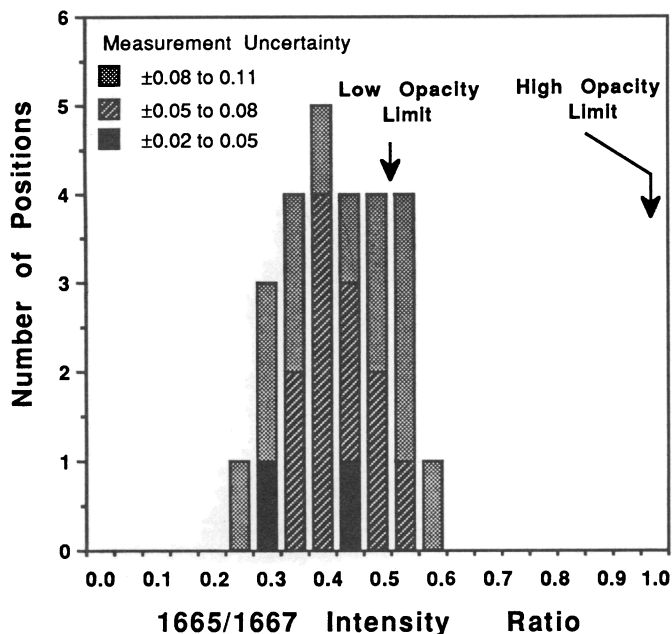


FIG. 2.—Histogram shows the distribution of the ratios of the 1665 and 1667 MHz OH lines, demonstrating that the lines have low opacity and that the intensities are not affected by possible, nonthermal excitation such as that sometimes seen to occur near bright infrared sources. The values cluster near the low-opacity limit of 0.56, with no values falling significantly away from the main cluster. The uncertainties in the ratios are calculated from the noise in the observed spectra, and the largest dispersion is seen for the noisiest spectra (dotted background), with uncertainties on the horizontal axis of ± 0.1 . The fact that the centroid of the distribution is actually slightly lower than the optically thin limit is not explained.

spectra by a factor 1.8, and performing a weighted average to minimize noise in the combined data.

The combined data (Fig. 3) show that the OH is generally seen in emission, with single velocity components corresponding to the CO line velocities. The sole exception occurs at the center of S255, where continuum emission from a bright embedded H II region created a complex absorption and emission spectrum. This spectrum will be discussed separately in a later paper. The line spectra were analyzed to determine the integrated intensity, mean velocity and velocity width. The results are given in Table 2, columns (4) to (6). Column (3) gives a qualitative indication of the location of the molecular cloud and of the CO boundary. Columns (7) to (9) give derived, column-averaged quantities and are discussed in § 4.

4. ANALYSIS

The present observations consist of emission line intensities of the 1665 and 1667 MHz spectral lines. Emission-line observations cannot provide column densities without some assumption about molecular excitation. Fortunately, for the 1665 and 1667 MHz OH lines, an adequate assumption is that the excitation temperature significantly exceeds the 2.7 K cosmic background temperature. Direct observational information is available from absorption-line observations toward background continuum sources. For example, Nguyen-Q-Rieu et al. (1976) have analyzed several sources. Their largest derived column density is toward 3C 123, where $\tau_{1667} \sim 0.06$ and $N_{\text{OH}} \sim 2.3 \times 10^{14} \text{ cm}^{-2}$, with $T_{\text{ex}} \sim 6 \text{ K}$ and $\Delta v_{\text{OH}} = 2.5 \text{ km s}^{-1}$. A similar and more extensive study (58 sources) is by

Dickey, Crovisier, & Kazès (1981). Their most opaque cloud was in front of 3C 111 ($\tau_{\text{H I}} \sim 1.0$), where they derive $\tau_{1667} \sim 0.18$ and $N_{\text{OH}} \sim 1.5 \times 10^{14} \text{ cm}^{-2}$, with $T_{\text{ex}} \sim 4.1 \text{ K}$ and $\Delta v_{\text{OH}} = 1.1 \text{ km s}^{-1}$. Our source list differs from those of Nguyen-Q-Rieu et al. and Dickey et al. in that the atomic halos of dense clouds are likely to have larger densities and, thus, higher excitation temperatures. Therefore OH column densities can be inferred directly from the integrated line intensities without any detailed knowledge about excitation.

4.1. Excitation and Line Formation

Accurate determinations of the OH column density require some knowledge of the physical parameters of the gas, which we take from our source models. We have corrected the derived OH column densities to account for the effects of the cosmic background radiation, and we have used a self-consistent physical/chemical model to infer a radial fractional abundance of OH, accounting for the observed/modeled radial distribution of molecular hydrogen. The OH distribution in terms of its radial abundance was derived from the modeling of the H I emission and an equilibrium chemistry code as discussed in an accompanying paper (Andersson & Wannier 1993, hereafter Paper VI), but the results are discussed in § 5.

One internal check on the rotational excitation is to

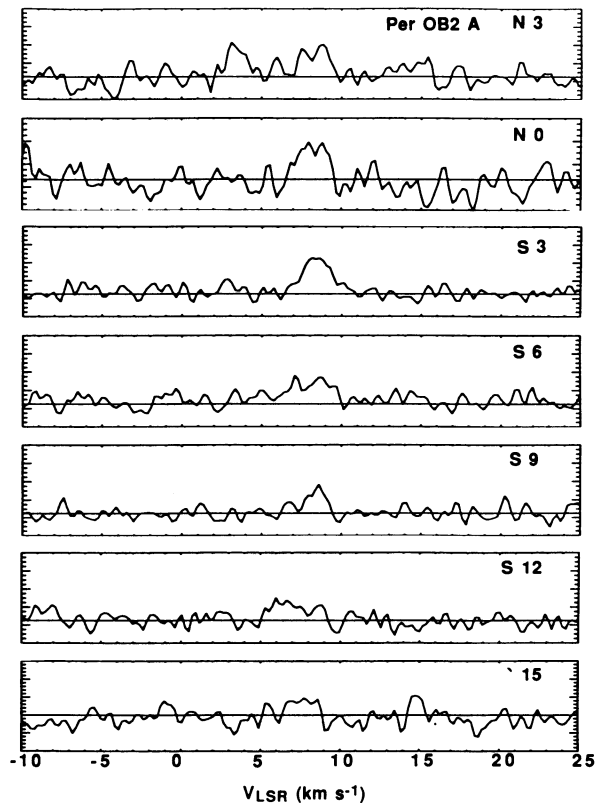


FIG. 3a

FIG. 3.—OH spectra are plotted for each position. Data from the two polarization states were combined and the 1665 and 1667 MHz data were co-added as described in § 3 to yield effective 1667 MHz line brightness temperatures. The horizontal velocity scale (V_{LSR} in km s^{-1}) is shown at the bottom of each figure and the vertical brightness scale (T_{A}^* in mK) is as follows: (a) -50 to 150, (b, c) -50 to 200, (d, e, f) -100 to 150, (g) -100 to 300, (h) -100 to 200, (i) -100 to 150, and (j) -150 to 250. In every case, the horizontal line is drawn at 0 mK, and each large division corresponds to 50 mK.

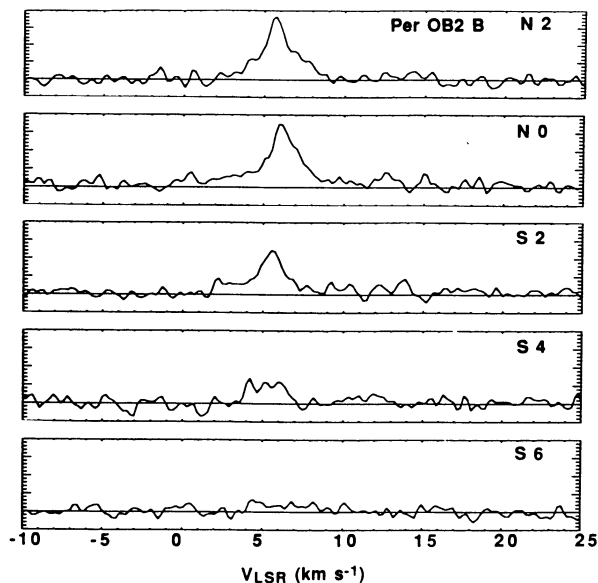


FIG. 3b

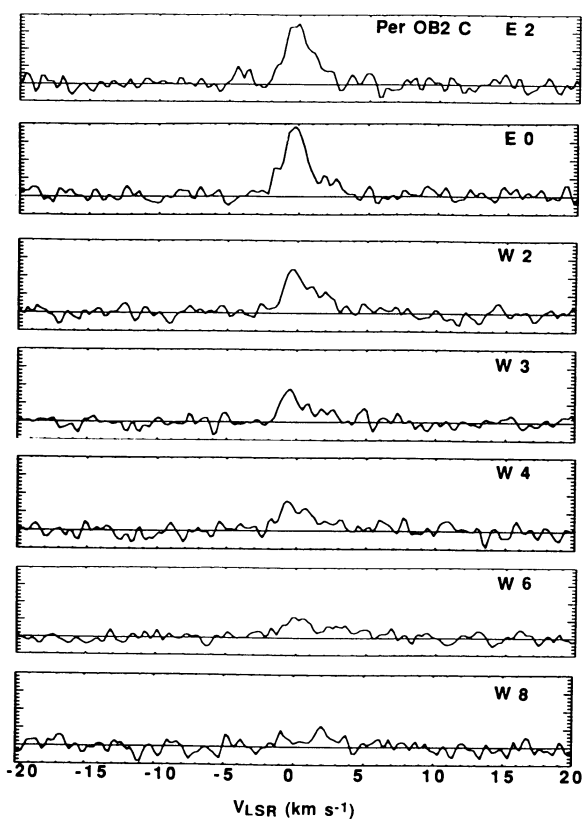


FIG. 3c

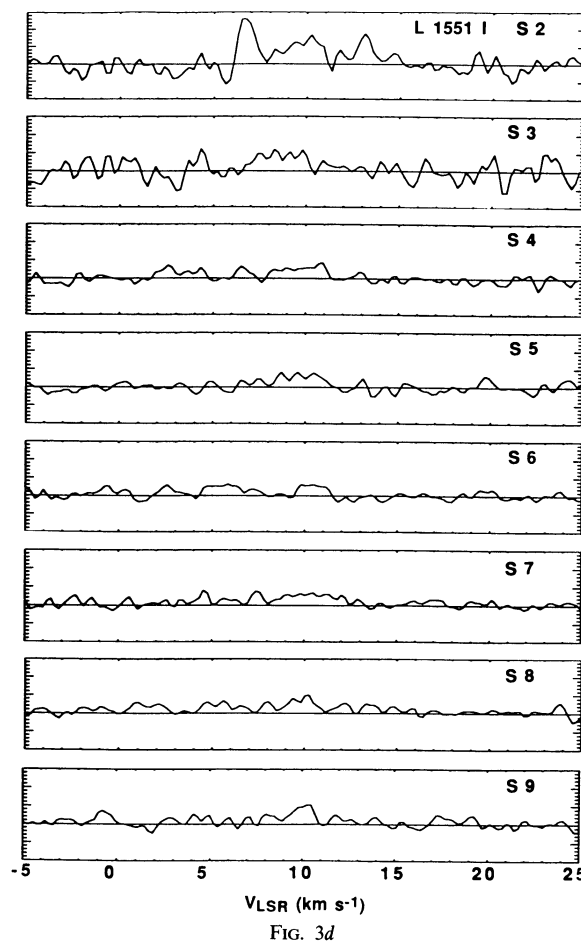


FIG. 3d

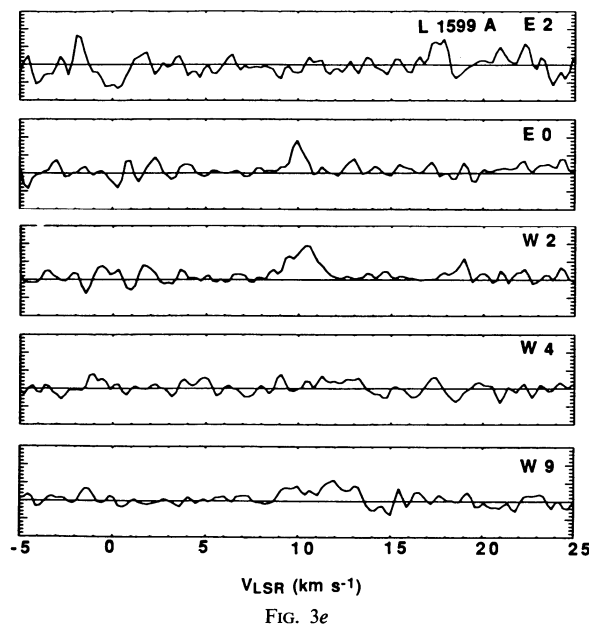


FIG. 3e

compare the 1665/1667 intensity ratio to theoretically predicted and previously observed values. The observations are shown in Figure 2, where the calculated ratios are weighted (by the stronger, 1667 intensity) intensity ratios, $R = \int I_{1665} \times I_{1667} dv / \int I_{1667} \times I_{1667} dv$, with the integral spanning the observable line profile. With typical errors in the ratio of ~ 0.1 , few are significantly different from the optically thin limit of 0.55 and none are even close to the optically thick limit of 1.00.

Interestingly however, the ratios cluster around an average of 0.4, smaller than the optically thin limit for thermalized excitation. Anomalies in the main-line ratios have been noted before (e.g., Crutcher 1979), though more commonly in the sense of the ratio being too large, rather than too small. Nevertheless,

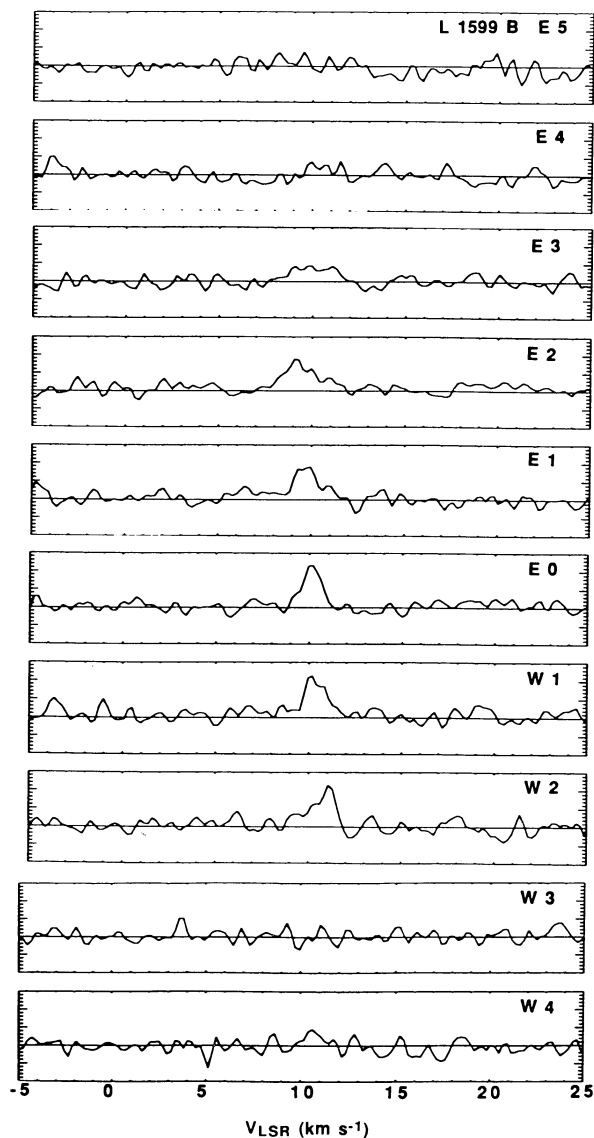


FIG. 3f

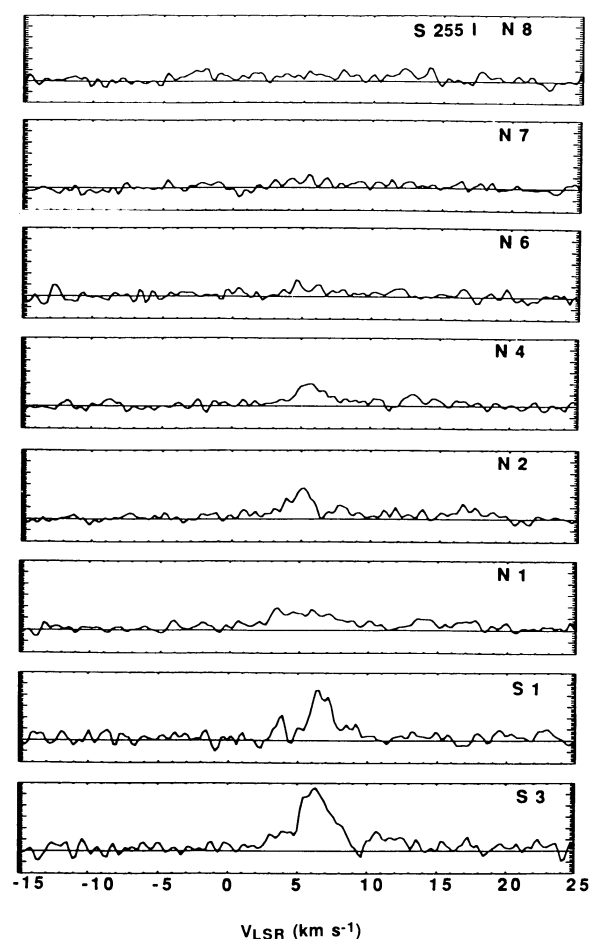


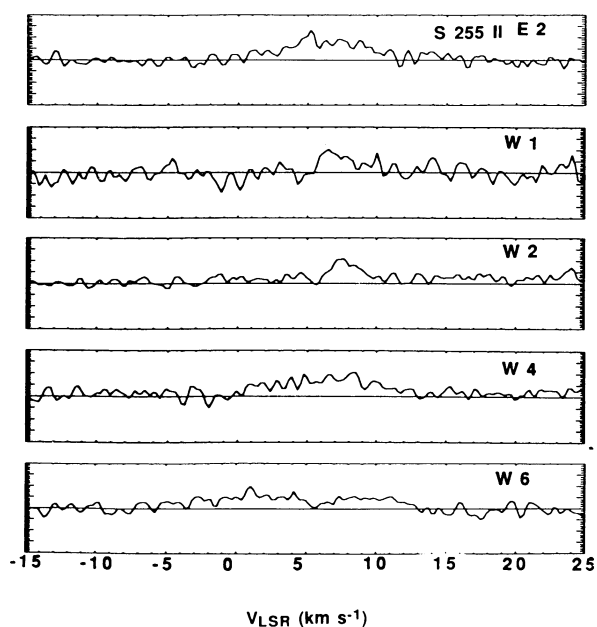
FIG. 3g

the present situation is not unprecedented, and reported instances of undersized ratios include prior observations of Per OB2 (Sancisi et al. 1974). In principle, it is possible that an excitation anomaly favoring the 1667 MHz line, could mask (partially cancel) an optically thick set of lines. However, in the cases which have been studied, including absorption-line observations to directly determine opacity, this never seems to occur and Crutcher (1979) concludes that undersized ratios “will not lead to any substantial underestimates of OH column densities”. For the purposes of the present paper, this is a sufficient conclusion.

Assuming that the two OH lines have intensities proportional to their statistical weights, the column density N_{OH} is related to the OH opacity by the relation

$$N_{\text{OH}} = C_0 \int T_{\text{ex}}(v) \times \tau(v) dv, \quad (1)$$

where C_0 is $2.2 \times 10^{14} \text{ cm}^{-2} (\text{K km s}^{-1})^{-1}$ for the 1667 MHz line and 4.0×10^{14} for the 1665 MHz line. The 1665 and 1667



VLSR (km s⁻¹)

FIG. 3h

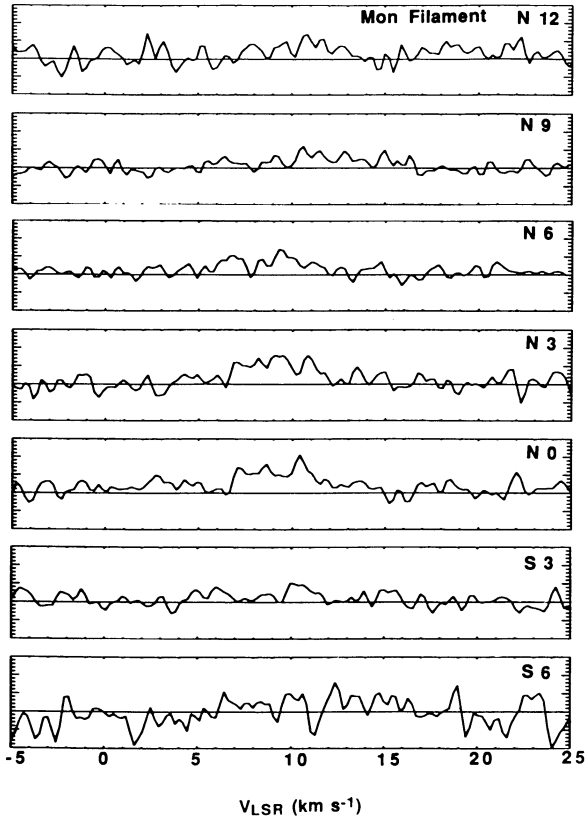


FIG. 3i

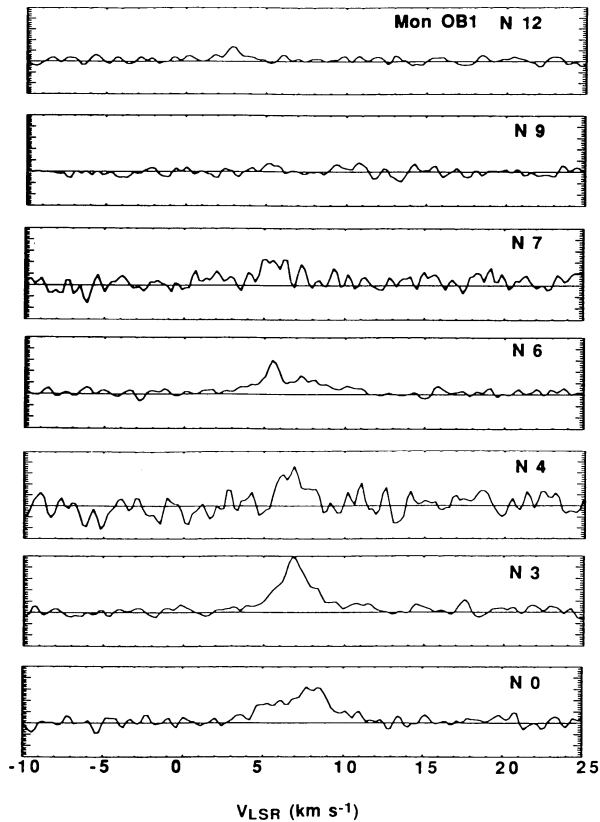


FIG. 3j

MHz lines appear to be optically thin, based on three lines of evidence: (1) the 1667/1665 intensity ratios in the present data are not smaller than the optically thin limit of 1.8 (Fig. 2), (2) the line intensities are very small compared to expected excitation temperatures, and (3) the cloud halos have similar characteristics to diffuse and translucent clouds which have been studied using absorption and emission lines and have been found to have $\tau(\text{OH}) \ll 1$ (cf. Dickey et al. 1981). In that case, for a source filling the main beam, we can write

$$N_{\text{OH}} = C_o \int T_A^*(v) [T_{\text{ex}} / (T_{\text{ex}} - T_{\text{bg}})] dv, \quad (2)$$

where T_A^* is the emission-line temperature, in excess of the background and corrected for the main beam efficiency η_b . If T_{bg} were negligible relative to T_{ex} then the column density is proportional to the integrated line intensity. For our sources, with $T_k \gg T_{\text{bg}}$, that becomes a question about LTE. We estimate the excitation temperatures for our sources from molecular parameters and from our source models, finding that $1 < T_{\text{ex}} / (T_{\text{ex}} - T_{\text{bg}}) \leq 1.3$ for all the gas, with values falling closer to unity for the bulk of the gas. In the Appendix we summarize the excitation processes for OH, which we used in our model calculations.

4.2. Physical Models of the Atomic Halos

In order to gain a better understanding of the atomic halos of molecular clouds we have developed a simple radiative transfer model for the H I and OH emission, using a physical model described in Papers IV and VI, and using model parameters fit to the H I and CO observations (but not the OH results!). The model is a dense spherical core of radius r_1 surrounded by an atomic halo of radius r_2 . The molecular excitation is assumed to be locally determined and the emergent intensity is found by direct integration of the transfer equation at each velocity, using thin concentric shells. The intrinsic line width is the root-sum-square of an assumed turbulent component, δv_{turb} , and the intrinsic thermal width. For comparison with observational data we output velocity-offset plots as well as traces of the peak temperature and integrated brightness temperature as functions of impact parameter. Absorption and emission spectra at a selected impact parameter are also produced.

The cloud parameters were chosen on the basis of H I and CO observations presented in Papers I and II and discussed in Paper III. For the observed clouds, values of r_1 were taken to be the outer limit of the CO cloud, and values of r_2 were determined from the H I data of Weaver & Williams (1973, hereafter WW). The H I column densities have been chosen to be compatible with preliminary VLA absorption-line observations, using extragalactic continuum sources in the direction of the clouds (Wannier, Andersson, & Moriarty-Schieven 1993). The density and temperature between r_1 and r_2 are power laws of the distance from the center of the cloud. Observations and modeling of the molecular component of interstellar clouds have shown that these can often be described as polytropes, typically of index about -3 ($n \propto r^{-3/2}$, $T \propto r^{1/2}$) (de Jong, Dalgarno, & Boland 1980; Dickman & Clemens 1983; van Dishoeck & Black 1986). The structure of polytropes of negative index has been described by Viala & Horedt (1974). For the H I halos, we find the most appropriate index to be ~ -1 ($n \propto r^{-1}$, $T \propto r^1$) (Paper VI). Table 3 lists the total extent of the halos as estimated from the H I emission. The S255 and Mon

TABLE 2
OH SPECTRA AND DERIVED COLUMN DENSITIES



















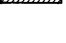














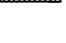
































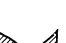




SOURCE DESCRIPTION			OBSERVED QUANTITIES			DERIVED QUANTITIES		
Strip Name (1)	Offset (HPBW) (2)	CO ? ^a (3)	$\int T_a^* dv$ (K km s ⁻¹) (4)	V_{LSR}^b (km s ⁻¹) (5)	Δv^b (km s ⁻¹) (6)	T_{ex} (K) (7)	N_{OH} (10 ¹⁴ cm ⁻²) (8)	$N_{OH}/N_{H I}^c$ (10 ⁻⁸) (9)
Per OB2 A ^d	n3		0.69 ± 0.14	8.0	6
	Center		0.43 ± 0.14	[8.1]	[4]
	s3		0.81 ± 0.11	8.5	5
	s6		0.70 ± 0.11	8.1	8
	s9		0.34 ± 0.11	[8.3]	[4]
	s12		0.51 ± 0.14	[6.9]	[8]
	s15		0.35 ± 0.19
Per OB2 B	n2		1.80 ± 0.11	5.8	6	15	4.4	2.6
	Center		1.79 ± 0.12	6.2	6	16	4.3	2.9
	s2		1.20 ± 0.10	5.5	6	17	2.9	2.4
	s4		0.66 ± 0.12	5.2	7	16	1.7	4.5
	s6		0.36 ± 0.10	[6.8]	[11]	17	0.9	2.4
Per OB2 C	se 2		1.86 ± 0.14	-0.1	6	14	4.5	5.1
	Center		2.20 ± 0.12	-0.2	6	16	5.3	6.6
	nw2		1.48 ± 0.10	0.2	17	17	3.6	5.2
	nw3		0.89 ± 0.11	-0.1	8	19	2.1	3.5
	nw4		1.00 ± 0.12	-0.0	9	19	2.4	4.9
	nw6		0.96 ± 0.10	0.6	10	18	2.3	10.8
	nw8		0.59 ± 0.13	1.3	11	16	1.4	6.9
L1551 I	s9		0.51 ± 0.10	9.9	6	27	1.2	6.5
	s8		0.59 ± 0.08	9.6	8	31	1.4	7.4
	s7		0.61 ± 0.10	9.9	11	34	1.4	7.5
	s6		0.43 ± 0.08	6.4	12	39	1.0	5.2
	s5		0.50 ± 0.10	9.4	7	43	1.2	5.0
	s4		0.75 ± 0.09	9.6	10	20	1.8	6.2
	s3		0.7 ± 0.2	9.1	8	18	1.6	9.1
	s2		1.7 ± 0.2	9.8	20	18	2.6	14.0
L1599 A	nw9		0.66 ± 0.12	11.6	10	17	1.6	9.6
	nw4		0.27 ± 0.12	[11]	[6]	20	0.6	1.9
	nw2		0.82 ± 0.12	1.6	4.3	17	2.0	2.7
	Center		0.41 ± 0.13	[10]	[2]	20	1.0	2.9
	se2		-0.2 ± 0.2	26	<0.9 ^e	<5.2 ^e
L1599 B	se5		0.21 ± 0.18	22	<1.3	<7.4
	se4		0.13 ± 0.14	27	<1.0	<5.1
	se3		0.52 ± 0.13	9.9	7	20	1.2	3.6
	se2		0.81 ± 0.11	9.3	6	18	1.9	3.0
	se1		0.75 ± 0.12	9.7	4	17	1.8	2.4
	Center		0.64 ± 0.11	10.1	3	16	1.5	2.0
	nw1		0.82 ± 0.13	10.2	4	17	2.0	2.6
	nw2		0.61 ± 0.13	10.6	4	18	1.5	2.3
	nw3		0.14 ± 0.15	20	<1.0	<3.1
	nw4		0.27 ± 0.16	27	<1.4	<7.2
S255 I	s3		3.3 ± 0.3	6.3	9	17	7.9	3.6
	s1		2.7 ± 0.2	6.7	7	17	6.5	3.0
	Center	
	n1		2.09 ± 0.14	5.2	15	17	5.0	2.4
	n2		2.0 ± 0.2	5.0	10	18	4.8	2.3
	n4		1.5 ± 0.2	5.8	9	22	3.5	1.9
	n6		0.8 ± 0.2	5.9	12	28	1.9	1.2
	n7		0.7 ± 0.2	5.6	12	34	1.6	1.2
	n8		1.0 ± 0.2	5.5	16	31	2.3	2.1
S255 II	e2		3.1 ± 0.2	6.4	19	17	7.4	3.3
	Center	
	w1		1.1 ± 0.2	7.6	8	19	2.6	1.3
	w2		1.7 ± 0.2	7.6	10	24	4.0	2.2
	w4		3.2 ± 0.2	6.8	22	31	7.4	6.7
	w6		2.8 ± 0.3	2.5	31	20	6.6	6.4
Mon filament	s6		0.6 ± 0.3	10	1.5	4.8
	s3		0.49 ± 0.14	[10.3]	[8]	28	1.1	3.6
	Center		1.42 ± 0.14	9.4	11	26	3.3	10.6
	n3		1.33 ± 0.16	9.1	11	26	3.1	9.9
	n6		0.98 ± 0.16	9.2	13	32	2.3	7.1
	n9		0.73 ± 0.13	11.4	11	10	1.9	5.7
	n12		0.91 ± 0.20	10.6	11	9	2.4	7.0
Mon I ⁸	Center		2.77 ± 0.15	7.6	11
	n3		2.75 ± 0.12	6.9	7
	n4		1.52 ± 0.33	6.8	5
	n6		1.75 ± 0.11	5.9	10
	n7		1.36 ± 0.29	5.6
	n9		0.10 ± 0.13
	n12		0.61 ± 0.10	2.9	8

TABLE 3
MODEL^a PARAMETERS

Strip Name	r_1 (pc)	r_2 (pc)	n_1 (cm ⁻³)	T_1 (K)	δv_{turb} (km s ⁻¹)
Per OB2 A
Per OB2 B	16.0	45	25	150	5.5
Per OB2 C	5.0	43	25	70	5.5
L1551 I	0.75	25	125	105	5.0
L1599 A	1.25	27	85	65	3.5
L1599 B	1.25	27	85	75	3.5
S255 I, II	18.0	75 ^b	105	190	12
Mon filament N	2.25	72	95	165	5
Mon filament S	2.25	22	95	165	5.5
Mon I

^a The model is a dense, spherical molecular core of radius r_1 surrounded by an atomic halo of radius r_2 ; n_1 and T_1 are the density and temperature of the atomic gas at r_1 and δv_{turb} is the assumed turbulent line width.

^b S255 has uncertain values of r_2 due to its location in the Galactic plane.

OB1 clouds lie close to the Galactic plane, making it more difficult to isolate the associated H I emission. In the case of S255, a halo-like structure was found after subtracting a background emission level, estimated from the data of WW, though its extent is probably overestimated because the proximity of S255 to the Galactic plane makes assignment of the H I gas difficult. No self-consistent solution to the coupled transfer-chemistry problem could be found for the large ($r_2 = 500$ pc) value implied by assigning all nearby H I gas to the cloud. Therefore, we set r_2 to 75 pc, the value for the Mon filament. No solution at all is given for Mon OB1 because the confusion problems are even worse than for S255. In one case, Per OB2 A, the CO has a tattered boundary, making an assignment for the location of the CO boundary dubious. In this case, we have also not made a detailed model.

The integrated H I intensity for each source was derived from the Arecibo H I data either directly or, in the case of obvious self absorption features, from Gaussian fits subtracting out the self-absorption. We used our transfer model to calculate the temperature of the halo, adjusting the density when needed. The procedure consisted of several steps: (1) with no background components added, find the amount of turbulence needed to achieve the observed line width, (2) add in the background components and vary n_1 and T_1 to fit the traces of T_p and $\int T$ while (3) adjusting the amount of cold "internal" H I needed to reproduce the observed self-absorption. For most sources this procedure leads to a reasonable and pretty much unique set of model parameters. The derived H I model parameters are given in Table 3.

^a The presence of CO at each map position is indicated by a box. The location of the CO boundary is indicated by a straight horizontal line. A wavy line indicates that the CO cloud extends beyond the present strip map.

^b When the determination of $\int T_p dv$ yields $0 < S/N < 2$, then velocity information is not given. When $2 < S/N < 4$, the error in derived V_{LSR} is estimated to be ± 1 km s⁻¹ and the error in Δv is ± 3 km s⁻¹ (square brackets). Otherwise the error in determining V_{LSR} is estimated to be ± 0.4 km s⁻¹ and the error in determining Δv is estimated to be ± 1 km s⁻¹.

^c $N_{\text{H I}}$ is taken from H I observations presented in the present paper and in Paper II together with source modeling.

^d Per OB2 A has an irregular CO profile in that it seems to pass through a clump beyond the molecular cloud boundary. As a result, we do not present a detailed cloud model for this source.

^e Inequalities are at 2σ confidence level.

^f In the center position of S255, there is a continuum source, OH absorption-line features and evidence for maser emission. Therefore, the derived line parameters are poorly defined.

^g Mon I is quite close to the Galactic plane and its extended H I envelope is not readily distinguishable from the general Galactic emission. Therefore we do not attempt to derive the OH fractional abundance.

4.3. OH Chemistry

In order to evaluate the OH results, we have compared the fractional abundances in Table 2 to the predictions of a chemical equilibrium calculation, using the physical model described in § 4.2. The chemistry code and reaction cross sections are those of Viala, Roueff, & Abgrall (1988; see also Viala 1986; Benayoun, Nercissian, & Viala 1991). The code was modified in a technical sense, to change from the original version operating on a Vax VMS machine (16-bit processing) to a version operating on a CRAY Y-MP (32-bit processing). This change produced no detectable difference (except in execution time!) in the output from several test runs made on both machines. Because the Viala et al. paper describes models run with certain variations in their input parameters, we list the input abundances in Table 4. Our values were chosen to be their "standard" values wherever possible, including their cosmic-ray ionization rate of 1.7×10^{-17} s⁻¹. The only significant modification to the Viala et al. parameters is the use of a reduced grain-formation rate for H₂, (Buch & Zhang 1991) motivated by our observations of H I in the halos (Paper VI). The chemistry calculations yield a steady-state solution for gas-phase abundances taking full account of the role of ionizing ultraviolet radiation. An outline of the key chemistry follows.

The hydroxyl radical is formed through two major reaction paths leading to formation of the molecular ion OH⁺. These start with the reaction of neutral oxygen and either H⁺ or H₃⁺. The chain involving H⁺ is endothermic by 0.0196 eV (227 K) and so has usually been considered unimportant in molecular clouds. Thus, in cool (<50 K) gas, OH formation involves a series of exothermic ion-molecule reactions (cf. Herbst & Klemperer 1973):

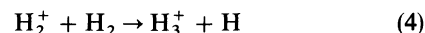
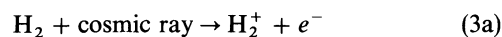
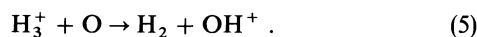


TABLE 4
INPUT ABUNDANCES

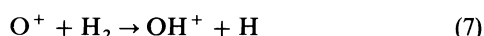
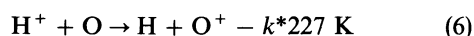
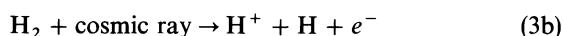
Element	Abundance
x_{He}	1.0×10^{-1}
x_{O}	5.0×10^{-4}
x_{C}	1.3×10^{-4}
x_{N}	6.3×10^{-5}
x_{S}	1.3×10^{-5}
x_{Mg}	1.4×10^{-6}
x_{Si}	8.3×10^{-7}
x_{Fe}	1.3×10^{-7}

and



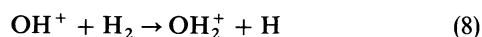
The space density of H_3^+ is usually taken to be $\sim 10^5 \text{ cm}^{-3}$, and more or less invariant with cloud density over a range from 10^4 to 10^7 cm^{-3} because the formation process per unit volume is linear with density and the destruction processes vary as the density squared. Recent laboratory measurements have affected the perceived recombination rate of H_3^+ (Adams & Smith 1987; Amano 1988) but probably do not profoundly affect the chemistry of OH (Viala 1986).

In warm interstellar gas, the path involving H^+ is more attractive:

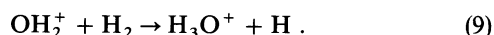


Below 50 K, reaction (6) is not significant since the rate constant decreases from $10^{-11} \text{ cm}^3 \text{ s}^{-1}$ to $10^{-19} \text{ cm}^3 \text{ s}^{-1}$ over the temperature drop from 50 to 10 K (Field & Steigman 1971).

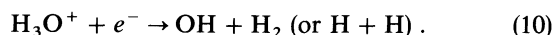
In either case, OH^+ is rapidly converted into H_3O^+ :



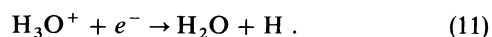
and



followed by dissociative recombination:

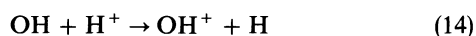
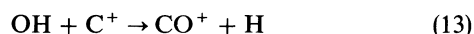


Doubt exists about the rate of reaction (10) in part due to an uncertain branching ratio with a major competing channel:

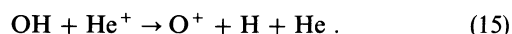


The fraction of recombinations leading to the formation of OH (reaction 10) has been variously taken as 50% (Herbst & Klemperer 1973), 80% (Herbst 1978), 67% (Viala 1986) and, recently, $\approx 0\%$ (Bates 1986; Lepp & Dalgarno 1987). Recently, a measurement of the channel leading to the production of OH (reaction [10]) has been made by Herd, Adams, & Smith (1990) leading to an estimate of its efficiency of $65 \pm 15\%$, the value used in our calculations.

The steady-state abundance of OH is determined by balancing the formation processes against the destruction, primarily by ions or energetic photons, namely



and



5. DISCUSSION

The 1665 and 1667 MHz lines are excellent tracers of OH column density, especially in the dense interiors of clouds where OH excitation temperatures are well in excess of the cosmic background temperature. Therefore, the observation that OH emission is extended beyond the CO cloud boundaries, and that OH emission is not sharply peaked toward the interiors of the clouds, indicate that OH exists predominantly

(with larger fractional abundance) in the lower density material near the H I halos. This conclusion becomes even more obvious by contrasting the smooth OH distribution to CO (and its isotopic forms) which show all the observed clouds to have centrally peaked molecular distributions.

The distinction between column density and fractional abundance is important. Although the column density of OH peaks in the direction of the very dense cores of the observed clouds (Table 2 and Fig. 4), it does so far less than would be expected if, for example, x_{OH} were held constant. This basic result is made more quantitative by making a three-dimensional model, including radially varying density, composition and temperature. The analysis is fully consistent in the sense that model OH and H I line emission is compared directly to the observations, and a chemistry code (including the effects of diffuse UV radiation) is used to model the H I and OH abundances.

The results of the model calculation in Figure 4 not only show the observed dip in fractional abundance near the boundary of the molecular cloud, but also reproduce quantitatively the observed OH abundance. The theoretical OH abundance was calculated without reference to the OH observations: i.e., no parameters were varied to match the observed intensities. The chemistry code and reaction cross sections are those of Viala et al. (1988), with the sole modification being the use of a reduced grain-formation rate for H_2 (Buch & Zhang 1991; Paper VI), as necessitated by previous H I (21 cm) observations. The remaining cloud model parameters are also taken from fits to our prior H I and CO observations, described in Paper VI. The model OH abundance in the halo is dependent

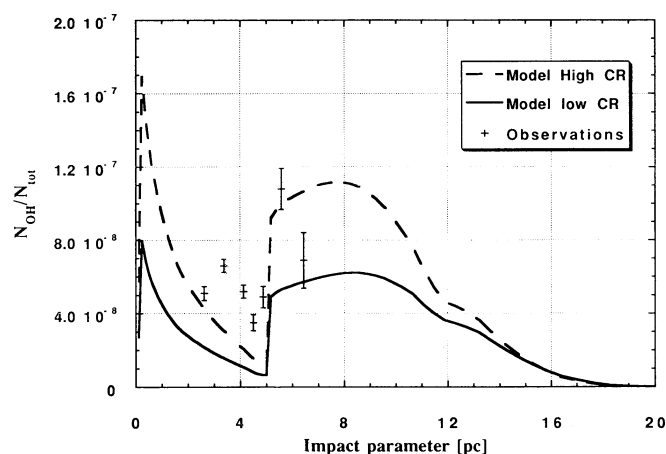


FIG. 4.—Comparison of theory and observations is presented for the OH abundance, x_{OH} , near the Per OB2 C molecular cloud edge. The theoretical OH abundance was calculated without reference to the OH observations (see § 4): i.e., no parameters were varied to match the observed intensities. The chemistry code and reaction cross sections are those of Viala et al. (1988), with the sole modification being the use of a reduced grain-formation rate for H_2 (Buch & Zhang 1991; Paper VI), as necessitated by previous H I (21 cm) observations. The remaining cloud model parameters are also taken from fits to our prior H I and CO observations, described in Paper VI. The rise in OH abundance beyond the CO edge is due to operation of the endothermic reaction $\text{H}^+ + \text{O} \rightarrow \text{H} + \text{O}^+$, driven by the high temperatures and UV fluxes in the halo. The two curves represent two different values of the assumed cosmic-ray flux. The larger value is from Glassgold & Langer (1974) and produces a hydrogen ionization rate, ξ_0 , of $1.5 \times 10^{-17} \text{ s}^{-1}$. The smaller value is half as large, and is that used by Viala (1986). As can be seen, both models produce the observed dip in OH abundance at 4 pc, and the implied cosmic-ray ionization rate is rather tightly confined.

on the assumed interstellar radiation field (ISRF) in the sense of decreasing with increasing ISRF. Happily, the standard ISRF reproduces quantitatively the observed OH abundance, and in a sense is confirmed by the present results. As is described in Paper VI, deviations from the standard ISRF are also difficult to reconcile with the H I observations reported in Paper II. In Figure 4, the two curves represent two different values of the assumed cosmic-ray flux. The larger value is from Glassgold & Langer (1974) and produces a hydrogen ionization rate, ξ_0 , of $1.5 \times 10^{-7} \text{ s}^{-1}$. The smaller value is half as large, and is that used by Viala (1986). As can be seen the implied cosmic-ray ionization rate is rather tightly confined.

The OH fractional abundance presented in column (9) of Table 2 is generally larger than would be expected, for example, from the models of Viala (1986). This can be understood in terms of (1) our larger, assumed kinetic temperatures (col. [5], Table 3), and (2) our decreased H_2 formation rate and resulting increase in H I (and H^+) column density. Both of these effects tend to drive the endothermic reaction of H^+ with O (reaction [6]), resulting in increased OH production. This result is supported in detail by scrutinizing the OH abundances in Table 2. The largest, inferred OH abundances (in excess of 6×10^{-8}) are found: beyond the CO edges of Per OB2 C, L1551 I, L1599 A, and S255 II, and throughout the Mon filament strip. Beyond the CO boundaries, the H^+ abundance rises rapidly, and the kinetic temperature slowly in our source models. The behavior in S255 is especially telling, since it is only in the EW strip, passing directly into the S254 H II region, that largest fractional abundances are seen. Likewise, in L1599 A, it is the northwest boundary, projecting into the λ -Ori H II region (S264) which shows a large OH abundance, rather than the southeast boundary. At this time, we have no clear explanation for the large abundances of OH seen throughout the Monoceros filament strip.

It is interesting to note that the same conditions (larger temperature and UV flux) indicated by the present OH observations, are also predicted, independently, from the CO and H I observations in combination with detailed source modeling (paper VI). Those results indicate that the standard grain-formation rate constant of H_2 ($3.6 \times 10^{-18} T^{0.5} \text{ cm}^3 \text{ s}^{-1}$), in combination with the standard interstellar radiation field (ISRF), cannot be reconciled with the H I observations. The transition from atomic to molecular hydrogen falls at too large a radius in these models and the resulting (modeled) H I emission is too flat as a function of offset from the clouds. A decrease in the assumed H_2 production rate has independent theoretical justification from the results of Buch & Zhang (1991), who showed that the sticking probability for hydrogen

atoms on ice grains can be smaller than unity by several orders of magnitude. The reduction in H_2 formation rate substantially increases the column density of the transition region (H I gas) and, because the far-UV is attenuated primarily by H_2 molecular lines, produces a much larger column density of warm H^+ needed to produce OH via reaction (6).

6. CONCLUSIONS

We have made 10 strip maps of 1665 and 1667 MHz OH emission, traversing the outer boundaries of five molecular clouds. The lines are optically thin and, based on our source models, the OH transitions are thermalized to temperatures well in excess of the cosmic background radiation. Therefore, we can directly infer the column density distribution of OH.

The OH emission is found to be significantly extended relative to CO, implying that OH is to be found in abundance in the shell of partly atomic, partly molecular gas surrounding the dense molecular clouds.

The fractional OH abundance is calculated using existing H I and CO observations, and detailed source models which include a complete chemistry network and a radiative transfer code. The largest OH fractional abundances are found outside of the CO clouds, especially in those regions thought to be suffused by intense UV radiation. Support for the importance of H^+ can be seen in two sources (S255 and L1599) in which the largest OH abundances are found where the molecular cloud adjoins a visible H II region.

We conclude that the extended OH is formed, not by the exothermic reaction of O with H_3^+ , but by the endothermic reaction, $\text{H}^+ + \text{O} \rightarrow \text{H} + \text{O}^+$. The increased importance of the endothermic channel, relative to that assumed in earlier work, results from (1) larger temperatures and (2) a larger column density of H I (and therefore H^+) due to the decreased efficiency of H_2 production. This is consistent with, and in fact predicted by, our earlier models based on H I and CO observations alone.

The research described in this paper was carried out in part by the Jet Propulsion Laboratory, California Institute of Technology, under a contract with the National Aeronautics and Space Administration. Computing support for this project was provided by the JPL Supercomputing Project, sponsored by JPL and the NASA Office of Space Science and Applications. This work was partially supported by the NAIC, which is operated by Cornell University under a management agreement with the National Science Foundation. One of us (B-G A.) wishes to acknowledge a generous grant from "Stiftelsen Blancheflor Boncampagni-Ludovisi, född Bildt."

APPENDIX

The excitation temperature for OH, T_{ex} depends on the ratio of the radiative deexcitation rate to the collisional de-excitation rate: $(A_{ul} + J \times B_{ul})/C_{ul}$. In this case, $J = 4\pi B_{\nu}(T)$, where $B_{\nu}(T)$ is the cosmic background radiation intensity. Assuming a background temperature of 2.74 K (Mather et al. 1990) and a molecular dipole moment of 1.6676 D, we derive $A_{ul} + J \times B_{ul} = 3.26 \times 10^{-8} \text{ s}^{-1}$ for the 1667 MHz line, dominated by stimulated emission. The 1665 MHz line is quite similar, except that it has a slightly smaller radiative rate.

The quantity C_{ul} depends on the fractional ionization $\chi (n_e/n_{\text{H I}} + 2n_{\text{H}_2})$ and, weakly, on T_k . A complete expression for $F(T_k)$ must include the separate temperature dependences for the neutral and electron excitation. For the electron collision rate, there is a factor $T_k^{-0.5} (3.35 + \ln T_k)$ (Bouloy & Omont 1977). For the neutral collisions, from an empirical fit to the data of Kaplan & Shapiro (1979) there is a factor $1.0 - \log^2 (T_k/40)$. Together these would yield

$$R = 5 \times 10^{-11} \{1.0 - \log^2 (T_k/40) + 1.1 \times 10^5 \chi [T_k^{-0.5} (3.35 + \ln T_k)]\} n_{\text{H I} + \text{H}_2}.$$

Following the discussion by Dickey et al. (1981) for neutral and electron collisions, we write

$$R = 5 \times 10^{-11} (1 + 1.1 \times 10^5 \chi) n_{\text{H I} + \text{H}_2} F(T_k), \quad (\text{A1})$$

and point out that $F(T_k)$ is a slowly-varying function, with $0.5 < F(T_k) < 1.0$ when $10 < T_k < 120$ K.

If $\chi = 0$ and $F(T_k) = 1.0$, then the 1667 MHz transition is sub-thermal ($T_{\text{ex}}/T_{\text{kin}} \leq 0.75$) when $n_{\text{H I}} + n_{\text{H}_2} \leq 5.0 \times 10^2 \text{ cm}^{-3}$, a condition which applies to the molecular cloud material (Guibert, Elitzur, & Nguyen-Q-Rieu 1978). Within the atomic halo itself, the electrons are mostly from C II. We assume a carbon gas-phase abundance of 1.6×10^{-4} (Jenkins & Shaya 1979), which we take to be equal to χ . Assuming $n_{\text{H}_2} \ll n_{\text{H I}}$ in the halo gas, equation (A1) becomes

$$R = 9.3 \times 10^{-10} n_{\text{H I}} F(T_k), \quad (\text{A2})$$

with the thermal excitation dominated by electrons, but at a rate proportional to the neutral density. Then, for the halo gas, the 1667 line will be subthermally excited whenever $n_{\text{H I}} \leq 26 \text{ cm}^{-3}$, a condition applying to some, but not all of our observations of the atomic halos.

REFERENCES

- Adams, N. G., & Smith, D. 1987, in IAU Symp. 120, *Astrochemistry*, ed. M. S. Vardya & S. P. Tarafdar (Dordrecht: Reidel), 1
- Amano, T. 1988, *ApJ*, 329, L121
- Andersson, B.-G., Roger, R. S., & Wannier, P. G. 1992, *A&A*, 260, 355 (Paper IV)
- Andersson, B.-G., & Wannier, P. G. 1993, *ApJ*, 402, 585 (Paper VI)
- Andersson, B.-G., Wannier, P. G., & Morris, M. 1990, *ApJ*, 366, 464 (Paper III)
- Baran, G. P. 1982, Ph.D. thesis, Columbia Univ.
- Bates, D. R. 1986, *ApJ*, 306, L45
- Benayoun, J. J., Nercissian, E., & Viala, Y. P. 1991, *Grenoble Obs. Internal Technical Astrophysics Memorandum* (1991, October)
- Bouloy, D., & Omont, A. 1977, *A&A*, 61, 405
- Buch, V., & Zhang, Q. 1991, *ApJ*, 379, 647
- Crutcher, R. M. 1973, *ApJ*, 185, 957
- . 1979, *ApJ*, 234, 881
- Cudaback, D. D., & Heiles, C. 1969, *ApJ*, 155, L21
- de Jong, T., Dalgarno, A., & Boland, W. 1980, *A&A*, 91, 68
- Dickey, J. M., Crovisier, J., & Kazés, I. 1981, *A&A*, 98, 271
- Dickman, R. L., & Clemens, D. P. 1983, *ApJ*, 271, 143
- Duerr, R., Imhoff, C. L., & Lada, C. J. 1982, *ApJ*, 261, 135
- Elias, J. H. 1978, *ApJ*, 224, 857
- Evans, N. J., Blair, G. N., & Beckwith, S. 1977, *ApJ*, 217, 448
- Federman, S. R., Evans, II, N. J., Willson, R. F., Falgarone, E., Combes, F., & Scheufele, B. M. 1987, *ApJ*, 322, 960
- Field, G. B., & Steigman, G. 1971, *ApJ*, 166, 59
- Glassgold, A. E., & Langer, W. D. 1974, *ApJ*, 193, 73
- Guibert, J., Elitzur, M., & Nguyen-Q-Rieu. 1978, *A&A*, 66, 395
- Herbst, E. 1978, *ApJ*, 222, 508
- Herbst, E., & Klemperer, W. 1973, *ApJ*, 185, 505
- Herd, C. R., Adams, N. G., & Smith, D. 1990, *ApJ*, 349, 338
- Heyer, M. H., Snell, R. L., Morgan, J., & Schloerb, F. P. 1989, *ApJ*, 346, 220
- Jenkins, E. B., & Shaya, E. J. 1979, *ApJ*, 231, 55
- Kaplan, H., & Shapiro, M. 1979, *ApJ*, 229, L91
- Lepp, B., & Dalgarno, A. 1987, *BAAS*, 18, 1029
- Maddalena, R. J., & Morris, M. 1987, *ApJ*, 323, 179
- Maddalena, R. J., Morris, M., Moscowitz, J., & Thaddeus, P. 1986, *ApJ*, 303, 375
- Magnani, L., & Siskind, L. 1990, *ApJ*, 359, 355
- Margulis, M., Lada, C. J., & Snell, R. L. 1988, *ApJ*, 333, 316
- Mather, J. C., et al. 1990, *ApJ*, 354, L37
- Moriarty-Schieven, G. H., Snell, R. L., Strom, S. E., Schlerb, F. P., Strom, K. M., & Grasdalen, G. L. 1987, *ApJ*, 319, 742
- Moriarty-Schieven, G. H., & Wannier, P. G. 1991, *ApJ*, 373, L23
- Murdin, P., & Penston, M. V. 1977, *MNRAS*, 181, 657
- Nguyen-Q-Rieu, Winnberg, A., Guibert, J., Lépine, J. R. D., Johansson, L. E. B., & Goss, W. M. 1976, *A&A*, 46, 413
- Perauld, M., Falgarone, E., & Puget, J. L. 1985, *A&A*, 152, 371
- Racine, R. 1968, *AJ*, 73, 233
- Sancisi, R., Goss, W. M., Andersson, C., Johansson, B., & Winnberg, A. 1974, *A&A*, 35, 445
- Sharpless, S. 1959, *ApJS*, 4, 257
- Snell, R. L. 1981, *ApJS*, 45, 121
- Snell, R. L., & Bally, J. 1986, *ApJ*, 303, 683
- Strom, S. E., Strom, K. M., Grasdalen, G. L., Capps, R. W., & Thompson, D. 1985, *AJ*, 90, 2575
- Strom, K. M., Strom, S. E., & Vrba, F. J. 1976, *A&A*, 81, 320
- Ungerechts, H., & Thaddeus, P. 1987, *ApJS*, 63, 645 (UT)
- van der Werf, P. P., Dewdney, P. E., Goss, W. M., & Vanden Bout, P. A. 1989, *A&A*, 216, 215
- van Dishoeck, E. F., & Black, J. H. 1986, *ApJS*, 62, 109
- Viala, Y. P. 1986, *A&AS*, 64, 391
- Viala, Y. P., & Horedt, G. P. 1974, *A&AS*, 16, 173
- Viala, Y. P., Roueff, E., & Abgrall, H. 1988, *A&A*, 190, 215
- Wannier, P. G., Andersson, B.-G., & Moriarty-Schieven, G. 1993, in preparation
- Wannier, P. G., Andersson, B.-G., Morris, M., & Lichten, S. M. 1991, *ApJS*, 75, 987 (Paper II)
- Wannier, P. G., Lichten, S. M., & Morris, M. 1983, *ApJ*, 268, 727 (Paper I)
- Weaver, H. F., & Williams, D. R. W. 1973, *A&AS*, 8, 1 (WW)